Title

Fluctuation-induced instabilities in front propagation up a comoving reaction gradient in two dimensions

Journal

Physical Review E, 74(1)

ISSN

1539-3755

Authors

Wylie, Christopher Scott
Levine, Herbert
Kessler, D A
et al.

Publication Date

2006-07-01

Peer reviewed

Fluctuation-induced instabilities in front propagation up a comoving reaction gradient in two dimensions

C. Scott Wylie* and Herbert Levine†
Center for Theoretical Biological Physics, University of California, San Diego, 9500 Gilman Drive, La Jolla, California 92093-0319, USA

David A. Kessler‡
Department of Physics, Bar-Ilan University, Ramat-Gan IL52900, Israel
(Received 4 April 2006; published 26 July 2006)

We study two-dimensional (2D) fronts propagating up a comoving reaction rate gradient in finite number reaction-diffusion systems. We show that in a 2D rectangular channel, planar solutions to the deterministic mean-field equation are stable with respect to deviations from planarity. We argue that planar fronts in the corresponding stochastic system, on the other hand, are unstable if the channel width exceeds a critical value. Furthermore, the velocity of the stochastic fronts is shown to depend on the channel width in a simple and interesting way, in contrast to fronts in the deterministic mean-field equation. Thus fluctuations alter the behavior of these fronts in an essential way. These effects are shown to be partially captured by introducing a density cutoff in the reaction rate. Moreover, some of the predictions of the cutoff mean-field approach are shown to be in quantitative accord with the stochastic results.

DOI: 10.1103/PhysRevE.74.016119 PACS number(s): 82.40.Ck, 02.50.Ey, 05.70.Ln

I. INTRODUCTION

Several well known processes in spatially extended systems exhibit fronts that propagate through space. Most of these processes that have been considered to date occur in media in which the governing dynamics are spatially uniform. Recently, however, some interesting findings have been made concerning fronts propagating in systems with spatially heterogeneous dynamics. In particular, the simple infection model $A+B\rightarrow 2A$ on a lattice with equal hopping rates and a linear reaction rate gradient has been studied [1,2]. Two versions of this system have been examined in some detail: one in which the gradient is defined with respect to the medium itself (the "absolute gradient"), and another in which the gradient is defined relative to the front's interface and travels along with the front (the "quasistatic gradient"). One can imagine numerous systems that can be described by the absolute gradient, e.g., a chemical reaction occurring in a temperature gradient, or a convection front [3] propagating in a system with nonparallel top and bottom plates. The quasistatic gradient is more analytically tractable and also arises naturally in models of biological evolution [4,5].

The usual way to analytically study a system with a propagating front, such as the infection model mentioned above, is within a mean-field (MF), reaction-diffusion framework. The simplest MF analog to our infection model is the well-known Fisher equation [6], with a spatially varying reaction rate:

$$\frac{\partial \phi}{\partial t} = D\nabla^2\phi + r(x)\phi(1-\phi). \tag{1}$$

For our simple infection model, Eq. (1) (the "naive MF") fails to capture many of the qualitative aspects of the stochastic problem with either absolute or quasistatic gradients. These failures, as well as many other issues involving the MF description of similar front propagation problems, are largely remedied [1,2,7–9] by introducing a cutoff factor in the reaction term [4,10,11]:

$$\frac{\partial \phi}{\partial t} = D\nabla^2\phi + r(x)\phi(1-\phi)\theta(\phi-\phi_c). \tag{2}$$

This added factor causes the reaction rate to abruptly drop to zero in regions far into the front's leading edge where ϕ drops below a critical level ϕ_c, and is meant to roughly mimic the effect of finite number fluctuations in the stochastic process. In other words, the discrete nature of individual particles implies that a sufficiently small value of the density field $\phi < \phi_c \sim 1/N$ corresponds, in an average sense, to zero particles present and thus zero reaction rate. In previous work [1,2], we showed how this modified MF treatment gives a quantitatively accurate prediction of the stochastic model in one dimension.

The purpose of this paper is to extend these investigations to the two-dimensional system. We will work in a channel geometry, with no-flux conditions on the sidewalls, such that the front propagates down the channel. In particular, we are interested in the patterns generated by the system, due to an instability to transverse fluctuations.

As mentioned previously, this system can be viewed as being analogous to certain problems in biological evolution.In this context, the relevant equation is similar to Eq. (2), but with a simpler rate term:

$$\frac{\partial \phi}{\partial t} = D\nabla^2\phi + (x-\bar{x})\phi\theta(\phi-\phi_c). \tag{3}$$

Here, ϕ represents the fraction of individuals in a population with a given fitness x. If the size of the population is fixed,

*Electronic address: cwylie@physics.ucsd.edu
†Electronic address: hlevine@ucsd.edu
‡Electronic address: kessler@dave.ph.biu.ac.il

the growth rate of individuals with a particular fitness is proportional to $x-\bar{x}$, where $\bar{x}$ is the mean fitness in the population. The diffusion term represents the effect of mutation, and the dynamics of the system corresponds to the population evolving towards greater mean fitness. The transverse y coordinate, being orthogonal to the fitness x, represents the frequency of some selectively neutral trait. Instability of a planar pulse would then correspond to evolution toward a nonuniform frequency distribution of this neutral trait. Due to the difference in the structure of the rate term, Eq. (3) describes an evolving *pulse* whereas Eq. (2) describes a *front*. However, this difference should not alter the stability properties of the system since, as we shall see, these properties are determined by the leading edge where the front and the pulse are identical. The cutoff term is appropriate in this context because members of a population, like particles, are quantized.

In this study, we focus our attention on the quasistatic gradient in two dimensions and ask how finite number fluctuations and the related cutoff approach affect the stability of planar fronts propagating in a rectangular channel. In what follows we will see that in contrast to the predictions of the naive MF, the results of stochastic simulations point to unstable planar fronts. Furthermore, once again the cutoff term will rescue the effectiveness of the mean field description of the stochastic process. We first study the cutoff mean-field equations, both numerically and analytically, showing the instability. We then turn to the stochastic model, demonstrating the instability there as well. An Appendix contains details about the numerics.

II. MEAN FIELD STABILITY CALCULATION

The full equation of motion governing the quasistatic gradient in the MF cutoff framework is Eq. (2) with

$$\phi(x,y,t) \equiv N_A/N,$$

$$r(x) \equiv \max[r_{min}, r_o + \alpha(x-\bar{x})],$$

$$\bar{x}(t) \equiv \frac{1}{b}\int \phi(x,y,t)dxdy,$$

$$\phi_c = k/N,$$

$$\partial_y \phi(x,0,t) = \partial_y \phi(x,b,t) = 0.$$

Here x is the direction parallel to the channel's long axis. N_A is the number of A's at a given site and N is the equilibrium

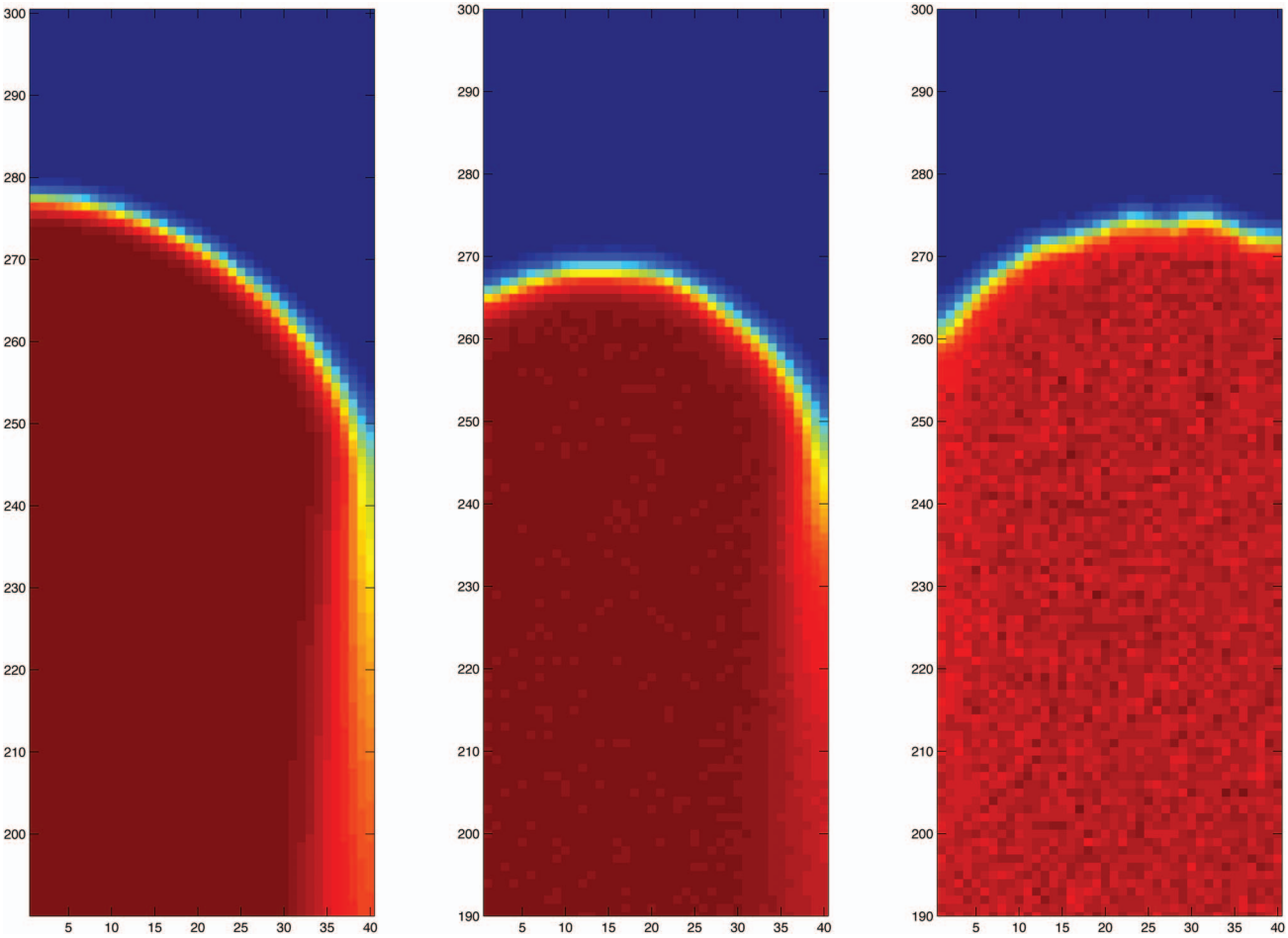

FIG. 1. (Color) Snapshots of the growing finger for the cutoff MF compared to that for the stochastic model. The parameters are $D=1$, $r_0=6$, $\alpha=0.3$. Lengths are expressed in units of the lattice spacing $l=1$. Left: The cutoff MF with $k/N=8.7\times10^{-5}$. Center: The stochastic model with $N=90801$. Right: The stochastic model with $N=2881$.

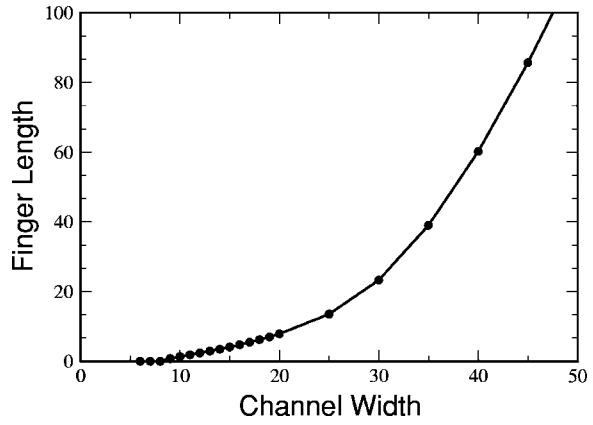

FIG. 2. Finger length (as defined in the text) versus channel width for the cutoff MF. The parameters are: $D=1$, $r_0=6$, $\alpha=0.3$, $k/N=8.7\times10^{-5}$, $l=1$.

number of A particles per lattice site. k is some $O(1)$ fitting parameter. $\bar{x}$ serves to define the interface position of the front by essentially comparing the front's profile to a step function, and b is the cross-channel width; note that the integral over x starts from $x=0$ which is the bottom of the computational domain. r_{min} merely serves to keep the reaction rate from going negative far behind the front and plays no role in the front dynamics.

To numerically investigate the stability of the planar front, we start with a front which is a slightly perturbed planar front, with

$$\phi(x,y,0) = \theta\left(10 + 0.01\cos\left(\frac{\pi y}{b}\right) - x\right) \tag{4}$$

with $\theta(x)$ again the Heaviside step function. Direct numerical integration of a spatially discretized version (with lattice spacing, l, unity) of the time-dependent Eq. (2) shows that planar fronts are in fact unstable to transverse fluctuations. For a sufficiently wide channel, perturbed planar fronts develop into long, though finite, fingers whose length increases with increasing channel width. An example of such a finger is shown in Fig. 1. We see that there is a deep narrow "notch" on the trailing side of the finger, so that the width of the interface is much greater here than for the rest of the finger. Defining the finger length by $\int[\phi(x,0)-\phi(x,b)]dx$, the data for finger length versus channel width is presented in Fig. 2. We now turn toward an analytic understanding of this result.

Due to the translational invariance of the system, it is natural to investigate first steady-state propagating planar front solutions. Plugging into Eq. (2) the traveling wave form, $\phi_0(x,y,t)=\phi_0(x-vt)$, with velocity v, we obtain

$$D\phi_0'' + v\phi_0' + r(z)\phi_0(1-\phi_0)\theta\left(\phi_0 - \frac{k}{N}\right) = 0 \tag{5}$$

in terms of the comoving coordinate $z\equiv x-vt$. An analysis of the linearized version of Eq. (5) provides insight into the role of the cutoff. As $z\to-\infty$, $\phi_0\to1$. Linearizing around $\phi_0=1$, we find two exponential solutions, but one must be discarded since it decreases with increasing z. Similarly, as $z\to\infty$, $\phi_0\to0$. Linearizing around $\phi_0=0$, in the region past the cutoff, once again we find only one acceptable, decaying solution. This leaves our solution with a total of two undetermined constants. Fixing translational invariance reduces this number to 1. Requiring continuity of ϕ_0 at the cutoff determines the remaining coefficient, and continuity of ϕ_0' determines the velocity. Thus, viewed mathematically, the cutoff fixes the velocity by overdetermining the boundary conditions, i.e., converting Eq. (5) into an eigenvalue problem. An analysis for large N yields the leading order result [1]:

$$v = [24D^2\alpha\ln(N/k)]^{1/3}. \tag{6}$$

In the limit $k/N\to0$ we regain the naive MF approach, in which $v\to\infty$. Thus the naive MF and the cutoff MF predict qualitatively different results for the velocity. Not surprisingly, stochastic fronts in fact approach a (finite) steady-state velocity that agrees well with that given by the cutoff MF.

Turning now to two-dimensional (2D) fronts, we wish to study the linear stability of the planar solution to transverse perturbations. We write $\phi(x,y,t)=\phi_0(z)+\tilde{\phi}(z,y,t)$ and linearize Eq. (2) with respect to $\tilde{\phi}$. The invariance of the system with respect to translations in time and the transverse spatial direction y implies $\tilde{\phi}(z,y,t)=e^{\omega t}e^{iqy}\eta(z)$. The governing equation for $\eta(z)$ is then

$$D\eta'' + v\eta' + \eta r(z)\left[(1-2\phi_0)\theta\left(\phi_0 - \frac{k}{N}\right) + \phi_0(1-\phi_0)\delta\left(\phi_0 - \frac{k}{N}\right)\right] = \Omega\eta \tag{7}$$

with

$$\Omega \equiv Dq^2 + \omega. \tag{8}$$

The delta function arises from differentiating the step function and is due to the shift in z_{cut} caused by the perturbation $\tilde{\phi}$. We have assumed here that $q\neq0$ so that $\int\tilde{\phi}(z,y,t)dy=0$. The case $q=0$ has to be treated separately and the linear operator is in fact different; but, for this sector the least stable mode is just the translation mode with $\Omega=0$. For the nonzero transverse wave vector, notice that Eq. (8) implies a simple stabilizing quadratic dependence of the growth rate ω on q. Thus the least stable mode is that with the smallest nonzero q, which, assuming a zero-flux sidewall boundary condition, is $q_{min}=\pi/b$. This implies a minimum channel width b^* below which even the longest wavelength mode has too much curvature for any instability to exist:

$$b^* = \pi\sqrt{\frac{D}{\Omega_{max}}}, \tag{9}$$

where Ω_{max} is the largest (positive) eigenvalue of the stability operator, Eq. (7).

Like the steady-state problem, insight can be gained into Eq. (7) by considering the boundary conditions at $z\to\pm\infty$. We require that $\eta\to0$ as $z\to-\infty$. As $\phi_0\sim1$ in this region, we find two exponential solutions for η: one growing with increasing $-z$ and the other decaying. The former must of course be excluded. If we perform the same procedure past

the cutoff, we find both modes decaying as $z \to \infty$. However, one of the modes decays more slowly than the steady-state solution and thus dominates it for sufficiently large z. This is unacceptable behavior for a perturbation and therefore this solution is discarded. Thus our solution has two arbitrary constants, one of which may be chosen arbitrarily since Eq. (7) is linear in η. The remaining constant is fixed by requiring continuity of η at the cutoff. Matching η' at the cutoff determines the eigenvalues Ω. Thus once again the cutoff has played a central role in determining the problem's interesting quantities.

As with the steady-state problem, we can make analytic progress in the limit of large N. In this case, the cutoff is at large z, in the region where ϕ_0 is small. If we consider Eq. (7) in the region where $\phi_0 \ll 1$ and $z < z_{cut}$, and fix the translation invariance by setting $\bar{z}=0$ for the unperturbed state, we obtain

$$D\eta'' + v\eta' + \eta(r_0 + \alpha z) = \Omega\eta. \tag{10}$$

Up to a similarity transformation, this is the Airy equation, with the general solution

$$\eta = e^{-vz/2D}\left[A\mathrm{Ai}\left(\frac{\Gamma - z}{\delta}\right) + B\mathrm{Bi}\left(\frac{\Gamma - z}{\delta}\right)\right] \tag{11}$$

with

$$\Gamma \equiv \frac{v^2/4D - r_0 + \Omega}{\alpha},$$

$$\delta \equiv \left(\frac{D}{\alpha}\right)^{1/3}. \tag{12}$$

We now can argue that the Bi term must vanish by considering the large v limit of Eq. (7) and matching onto Eq. (11). As shown in Ref. [2], in the large v limit, the diffusion term in Eq. (10) can be ignored, and the solution in the region where $\phi_0 \ll 1$ is

$$\eta \sim e^{-(1/v)[(r_0-\Omega)z+(1/2)\alpha z^2]}. \tag{13}$$

Expansions of Ai and Bi for a large argument show that the diffusionless result Eq. (13) matches onto Eq. (11) only if the Bi term is absent. The constant A may be arbitrarily set to unity since the problem is linear. Thus we have for $z \lesssim z_{cut}$

$$\eta = e^{-vz/2D}\mathrm{Ai}\left(\frac{\Gamma - z}{\delta}\right). \tag{14}$$

We have to match this result to the simple exponential solution for $z > z_{cut}$. Thus

$$e^{-vz_{cut}/2D}\mathrm{Ai}\left(\frac{\Gamma - z_{cut}}{\delta}\right) = Ce^{[-(vz_{cut}/2D)(1+\sqrt{1+4\Omega_0 D/v^2})]}. \tag{15}$$

The derivative of η must also match properly at the cutoff. Looking back to Eq. (7), we see that the delta function term causes a discontinuity in η' at z_{cut}:

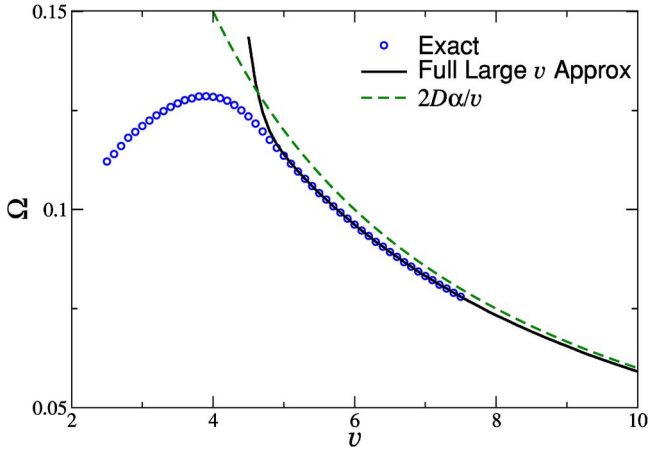

FIG. 3. (Color online) The circles represent the exact numeric solution of Eq. (7). The solid line is the exact numeric solution of Eq. (17) which is itself a large v approximation. Exact numerically generated values of N and z_{cut} were used to generate this approximation. The dashed curve is the analytic approximation Eq. (19). The parameters are $D=r_0=1$, $\alpha=0.3$.

$$\frac{\eta'_{right} - \eta'_{left}}{\eta(z_{cut})} = \frac{r(z_{cut})}{D}\frac{(k/N)(1-k/N)}{\phi_0'(z_{cut})} = -\frac{r(z_{cut})}{v}(1-k/N). \tag{16}$$

Computing the derivatives, we obtain

$$\frac{v}{2D}\sqrt{1+4D\Omega/v^2} - \frac{1}{v}(r_0 + \alpha z_{cut})(1-k/N) = \frac{1}{\delta}\frac{\mathrm{Ai}'([\Gamma(\Omega) - z_{cut}]/\delta)}{\mathrm{Ai}([\Gamma(\Omega) - z_{cut}]/\delta)}. \tag{17}$$

This equation determines Ω if the quantities v and z_{cut} are known.

For large v, we can progress further by noting that the left-hand side of Eq. (17) is also large. For the right-hand side to balance it, the Airy function in the denominator must be small. Thus $\frac{\Gamma - z_{cut}}{\delta} \approx \xi_0$, where $\xi_0 \approx -2.3381$ is the first zero of the Airy function. For the position of the cutoff, we quote another result from Ref. [1] obtained by matching the linearized steady-state equation at the cutoff:

$$z_{cut} \approx \frac{v^2/4D - r_0}{\alpha} - \xi_0\delta - \frac{2D}{v}. \tag{18}$$

Plugging this expression into Eq. (17), expanding around ξ_0, and dropping higher order terms, we obtain the leading order result valid for large v:

$$\Omega = \frac{2D\alpha}{v}. \tag{19}$$

This result is tested in Fig. 3, where we plot the eigenvalue Ω versus velocity determined by an exact numerical solution of Eq. (7), together with the numerical solution of the matching condition, Eq. (17), and the leading-order result, Eq. (19). We see that indeed the leading-order result approaches the exact result as v increases.

Our leading-order result, Eq. (19), yields the interesting conclusion that planar fronts become stable in the limit as $v \to \infty$, i.e., $N \to \infty$, i.e., the cutoff disappears. Equation (19) can be interpreted as saying that Ω is proportional to the ratio of the diffusive length scale (D/v) to the length scale over which the rate changes appreciably $(1/\alpha)$. Thus heuristically incorporating the effects of finite number fluctuations qualitatively changes the system's stability properties by limiting the front's velocity, which in turn makes the diffusive length scale finite. In practice, however, without a cutoff, an initial front which is compact (or decays sufficiently rapidly) will act as a time-dependent cutoff [12], so that at least initially transverse fluctuations will grow. The fluctuation induced instability in this system is similar to that in Ref. [11], where it was found that a coupled reaction diffusion system with no reaction gradient, but with unequal diffusion coefficients, is unstable with a cutoff but stable without one. Furthermore, Eq. (19) shows that the fronts become stable as $\alpha \to 0$, for any value of N. This is consistent with the stability shown in Ref. [11] in the case of equal diffusion coefficients.

Thus, once again, the presence of the cutoff qualitatively changes the simple mean field predictions. If the cutoff approach indeed captures the effect of finite number particle fluctuations, we should expect to see some analog of this front instability in the stochastic, discrete infection model discussed earlier, to which we now return.

III. STOCHASTIC SYSTEM

We ran simulations in which the lower rectangular portion of the channel was initially populated with N particles of type A per lattice site and the upper rectangular portion of the channel was populated by N particles of type B per lattice site. During each time step, a binomially distributed random number of particles hop to adjacent sites. Furthermore, A particles probabilistically cause some B particles to change into A particles. The reaction probability and hopping rates were chosen so that the discretized, stochastic equation for ΔN_A reduces to Eq. (1) [with the quasistatic form for $r(x)$] when the expectation value is taken in the small time, small lattice spacing limit. In particular, for the hopping probability we took $P_{hop} \sim D\frac{dt}{l^2}$, where dt is the simulation time step and l is the lattice spacing. The number of particles reacting during each time step was chosen as a binomially distributed random variable characterized by N_A repetitions of a Bernoulli process with individual event probability given by $1-\left(1-\frac{r(x)dt}{N}\right)^{N_B}$.

The simulation results are easiest to interpret when the channel width b and the average number of particles per lattice site, N, are large. For fixed large N, there is some b beyond which there is a pronounced finger which survives for very long times. An example of such a finger is seen in the middle frame of Fig. 1. The overall similarity of the patterns for the MF simulation and the stochastic one is clear. As N is reduced for the same b, the statistical fluctuations become larger, as expected, and give the finger a clearly finite lifetime before it succumbs to the noise. The pattern eventually regenerates, sometimes with opposite parity, and the cycle of destruction and regeneration starts anew. Such a noise-roughened finger in seen in the rightmost frame of the figure; here N was chosen to correspond to the cutoff chosen for the MF simulation seen in the leftmost frame. The very visible effect of the noise is striking given the still quite large value of N employed, underscoring the extreme sensitivity of our system to fluctuations.

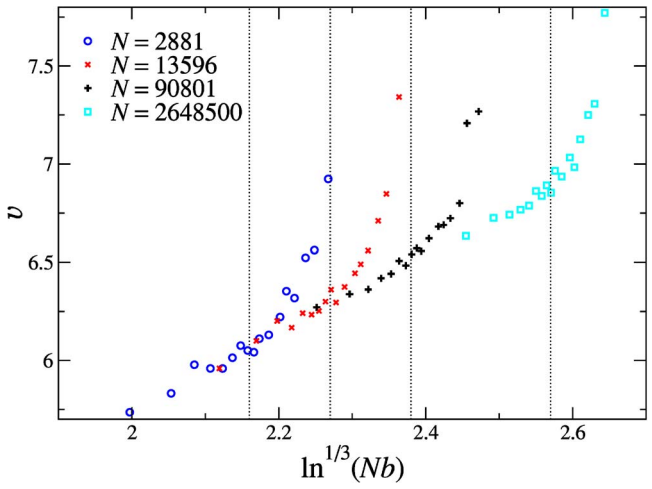

FIG. 4. (Color online) Evidence of the transition to instability. The linear envelope of the different curves demonstrates the N renormalization $N_{eff} \sim Nb$ required by widening the channel. The dotted lines show the b^* resulting from the corresponding deterministic, MF cutoff simulation ($k=0.25$). Each data point represents an ensemble average of three long trials (100 time units each). The parameters are $D=1$, $r_0=6$, $\alpha=0.3$, $l=1$.

For very narrow channels, on the other hand, the interface appears to be essentially planar, with random short-lived fluctuations. All this is in accord with our expectations based on our study of the cutoff MF dynamics. What is more subtle, however, is a quantitative measurement of the critical value of b for the onset of the pattern. On the small b side of the transition, the pattern is not exactly planar due to noise. On the large b side, the pattern is smeared out due to noise. This problem is exacerbated by the supercritical nature of the transition, such that the pattern has very small amplitude near the transition. In order to compare the stochastic system to the MF prediction, we need a way to distinguish this random roughening of the interface from the genuine pattern forming mechanism discussed in the previous section. We present below two tests whose results we believe demonstrate the existence of a sharp transition in the stochastic system.

Both of these tests exploit the predicted transition between stable and unstable states that occurs when the channel width exceeds a critical value b^*, as stated in Eq. (9). First, we measured the ensemble averaged velocity of the mean interface $\bar{z} \equiv \Sigma_{i,j} \frac{A(i,j)}{Nb}$ as a function of b (Fig. 4). The increasing trend along the envelope of the different curves can be understood as a result of wider interfaces presenting an effectively larger number of particles N_{eff}. In fact, since in the steady state, $v \sim (\ln N)^{1/3}$, we see from the figure the remarkably simple result $N_{eff} \sim Nb$. This simple dependence continues until b approaches b^* (dotted vertical lines), where the

velocity suddenly increases. This increase can be understood as a result of the system spending much of its time in a configuration in which one side of the interface significantly leads in front of the other. The lagging side then effectively stalls while the leading side is in a region of large reaction rate, and thus propagates quickly. The overall effect is an increase in the velocity averaged over the width of the channel. The fact that the change occurs so near the b^* calculated earlier suggests that the cutoff approach is effectively capturing the stochastic dynamics.

As a second test, we plot the mean roughness of the interface W vs b (Fig. 5). W is defined in the standard way,

$$W^2 \equiv \left\langle \left\{ \left[\sum_j A(i,j)/N \right] - \bar{z} \right\}^2 \right\rangle,$$

where $\langle\rangle$ denotes ensemble average and the bar denotes average over the transverse direction. For $b < b^*$ we see power law scaling reminiscent of that discovered by Kardar, Parisi, and Zhang [13] for a growing interface. However, the data show no sign of a universal exponent. It may be that the very weak stability of the interface near b^* is responsible for a long crossover. This issue clearly requires more extensive study. For a fixed b, W decreases with increasing N, consistent with the hypothesis that interface roughness is noise driven in this regime. However, for $b \gtrsim b^*$ this simple dependence is lost. The curves converge near b^*, showing that particle number and its associated noise are no longer the relevant factor in determining interface roughness. Past this intersection, there is no apparent correlation between W and N. We interpret this as a crossover from noise driven interface roughness to gradient driven pattern formation occurring very near the b^* predicted from the cutoff MF approach.

Thus the cutoff MF approach is quantitatively successful in predicting the transition of the width and velocity observed in ensemble averaged stochastic fronts when the channel is widened. In contrast, the naive MF approach predicts no such transition and an infinite steady-state velocity, in stark qualitative disagreement with the simulation results. The cutoff MF approach also predicts the velocity of the average interface for $b < b^*$, provided we take $N \to Nb$.

Another aspect of the stochastic system which one would like to predict is the ensemble-averaged shape. We find that qualitatively this behaves as expected; namely, for small channel width the average shape is flat, and above the critical width, a nontrivial shape is apparent. The amplitude of the averaged pattern continues to increase with increasing width. However, we do not know how to quantitatively relate the average pattern to the results of the cutoff MF equations. One obvious impediment is the fact that the stochastic system switches parity at random, with the right and left sides alternating as the leading edge. Thus a naive ensemble average produces a shape which is highest in the center, clearly at odds with the deterministic calculation. Another aspect of the problem that we would like to correlate with the deterministic calculation is the growth rate of the pattern near onset. This problem is also difficult because the width, measured in the usual way, consists of a contribution from noise driven roughening and one due to pattern formation. Clearly, the usual MF approach can only make predictions about the contribution due to pattern formation and thus the stochastic results and MF predictions are intrinsically difficult to compare. Even though the noise decreases with increasing N, the dominance of the dynamics by the leading edge where fluctuations are unavoidably present makes this a nontrivial task, even at large N. These questions remain challenges for the future.

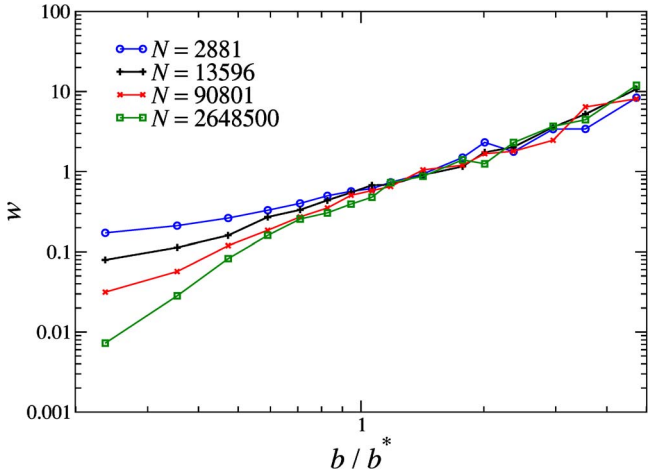

FIG. 5. (Color online) Noise driven roughness scaling for $b < b^*$, gradient driven scaling thereafter. Each data point represents an ensemble average of three long trials (100 time units each). Parameters are $D=1$, $r_0=6$, $\alpha=0.3$, $l=1$.

ACKNOWLEDGMENTS

The work of H.L. and C.S.W. was supported in part by the NSF PFC-sponsored Center for Theoretical Biological Physics (Grant No. PHY-0216576 and Grant No. PHY-0225630). The work of D.A.K. was supported in part by the Israel Science Foundation.

APPENDIX: DETAILS CONCERNING THE NUMERICAL INTEGRATION

In order to determine the spectrum $\Omega(v)$ we numerically integrated Eq. (7), and this required numerically integrating Eq. (5). Integration of Eq. (5) was initialized in the bulk state, from the left, where we defined $z \equiv 0$. We set v arbitrarily, took $\phi_0(0)=0.99$, and calculated $\phi_0'(0)$ from the solution to the version of Eq. (5) linearized around $\phi_0 \approx 1$,

$$\phi_0'(0) = -\frac{0.01v}{2D}\left(-1+\sqrt{1+\frac{4Dr_{init}}{v^2}}\right).$$

r_{init}, which we set to one, differs from the previously defined r_0 in that it fixed the rate at a definite location in the bulk state rather than the location where $\phi_0=1/2$. Integration terminated in the neighborhood of the cutoff, half way between time steps where ϕ_0'/ϕ_0 crosses $-v/D$. N was then read off from the relation $N=-\frac{vk}{D\phi_0'(z_{cut})}$ and the value of the cutoff was recorded for subsequent numerics. This value is measured relative to the bulk position where $\phi_0=0.99$, not relative to $\bar{z}$,

where $\phi_0=1/2$. All of this was done using ode45 from MATLAB, with a maximum step size of 0.001.

The solution for ϕ_0 appears as a coefficient in Eq. (7), and was incorporated into the ordinary differential equation (ODE) integration scheme with a cubic spline. Numerical integration of Eq. (7) was initialized at $z=0$ with some trial Ω_0, $\eta(0)=1$, and

$$\eta'(0)=\frac{v}{2D}\left(-1+\sqrt{1+\frac{4D(r_{init}+\Omega_0)}{v^2}}\right)$$

which follows from Eq. (7) if we plug in $\phi_0\approx 1$. Integration terminated at the z_{cut} obtained from integration of Eq. (5), where we checked if Eq. (16) was satisfied with the trial Ω. This procedure was iterated with a root solver while varying Ω until Eq. (16) was satisfied. Each integration of Eq. (7) was done over 1000 time steps with a fourth order Runge-Kutta ODE solver with fixed step size, meant to facilitate incorporation of the spline.

This yields the exact numeric solution presented in Fig. 3. Our "exact analytic approximation" presented in Fig. 3 is just the solution to Eq. (17) obtained with a root solver. The required values for N and z_{cut} were obtained from the previous integration of Eq. (5), and we took $r_0=1$. Since we dropped the term involving ϕ_0 in Eq. (10), this equation is insensitive to the precise definition of $\bar{z}$, e.g., it could be defined naturally as the coordinate where $\phi_0=1/2$ or it could be defined out of numerical convenience as the coordinate where $\phi_0=0.99$. This insensitivity explains why the results agree so well despite the fact that r_0 and r_{init} are not defined in the same way.

[1] E. Cohen, D. A. Kessler, and H. Levine, Phys. Rev. E **72**, 066126 (2005).

[2] E. Cohen, D. A. Kessler, and H. Levine, Phys. Rev. Lett. **94**, 158302 (2005).

[3] J. Fineberg and V. Steinberg, Phys. Rev. Lett. **58**, 1332 (1987).

[4] L. S. Tsimring, H. Levine, and D. A. Kessler, Phys. Rev. Lett. **76**, 4440 (1996).

[5] I. Rouzine, J. Wakeley, and J. Coffin, Proc. Natl. Acad. Sci. U.S.A. **100**, 587 (2003).

[6] R. A. Fisher, Annals of Eugenics **7**, 355 (1937), available at http://digital.library.adelaide.edu.au/coll/special/fisher/152.pdf

[7] E. Cohen, D. A. Kessler, and H. Levine, Phys. Rev. Lett. **94**, 098102 (2005).

[8] E. Cohen, D. A. Kessler, and H. Levine, Phys. Rev. E **73**, 016113 (2006).

[9] E. Cohen and D. A. Kessler, J. Stat. Phys. **122**, 925 (2006).

[10] E. Brunet and B. Derrida, Phys. Rev. E **56**, 2597 (1997).

[11] D. A. Kessler and H. Levine, Nature (London) **394**, 556 (1998).

[12] D. A. Kessler, Z. Ner, and L. M. Sander, Phys. Rev. E **58**, 107 (1998).

[13] M. Kardar, G. Parisi, and Y.-C. Zhang, Phys. Rev. Lett. **56**, 889 (1986).